TOPOLOGICAL ZEEMAN EFFECT AND CIRCULAR BIREFRINGENCE IN TWISTED PHOTONIC CRYSTAL FIBERS

T. Weiss,[1,*] G. K. L. Wong,[1] F. Biancalana,[1,2] S. M. Barnett,[3] X. M. Xi[1] and P. St.J. Russell[1,4]

[1]Max Planck Institute for the Science of Light, Guenther-Scharowsky Str. 1, 91058 Erlangen, Germany

[2]School of Engineering & Physical Sciences, Heriot-Watt University, Edinburgh, EH14 4AS, UK

[3]Department of Physics, University of Strathclyde, Glasgow G4 0NG, UK

[4]Department of Physics, University of Erlangen-Nuremberg,
Guenther-Scharowsky Str. 1, 91058 Erlangen, Germany

[*]Corresponding author: thomas.weiss@mpl.mpg.de

Abstract

The propagation of light guided in optical fibers is affected in different ways by bending or twisting. Here we treat the polarization properties of twisted six-fold symmetric photonic crystal fibers. Using a coordinate frame that follows the twisting structure, we show that the governing equation for the fiber modes resembles the Pauli equation for electrons in weak magnetic fields. This implies an index splitting between left and right circularly polarized modes, which are degenerate in the untwisted fiber. We develop a theoretical model, based on perturbation theory and symmetry properties, to predict the observable circular birefringence (i.e., optical activity) associated with this splitting. Our overall conclusion is that optical activity requires the rotational symmetry to be broken so as to allow coupling between different total angular momentum states.

OCIS Codes: 060.0060 Fiber optics and optical communications, 260.0260 Physical optics,
220.0220 Optical design and fabrication

Introduction

Field Code Changed
Field Code Changed
Field Code Changed

Permanently twisted photonic crystal fibers (PCFs) exhibit a number of interesting features, including the appearance of twist-tunable dips in their transmission spectra [1,2]. These are caused by the appearance at specific wavelengths of eigenmodes consisting of superpositions of core and leaky ring-shaped cladding modes [1]. Twisted PCFs also show highly reproducible levels of optical activity (i.e., circular birefringence) in the spectral windows between these dips [3]. Although several theoretical and experimental papers have treated twisted fibers in various different contexts [4-7] and stress-induced circular birefringence has been studied in twisted single-mode step-index fibers [8,9], detailed analysis of more complex twisted fiber systems is still missing. In unstressed twisted fibers, a helically twisting fiber axis or a birefringent core is often considered a prerequisite for the observation of optical activity. In this paper we show, however, that pure optical activity can be induced in fibers with zero linear birefringence provided the core has a non-circular cross-section, such as is the case in a hexagonally structured (six-fold rotationally symmetric) PCF, or a step-index fiber with a perfectly square (four-fold rotationally

symmetric) core. At this point, it should be emphasized that a non-circular core does not in general imply birefringence [10,11]. In fact, any core with n-fold rotational symmetry has zero birefringence for $n>2$ [12,13].

Formatted: Font: Italic

The purpose of this paper is thus to analyze in detail the recently reported experimental results on optical activity in twisted PCFs [3]. By solving Maxwell's equations in a twisted frame, we present a polarization-dependent theory of light propagation in these fibers. The governing equation turns out to resemble the Pauli equation for electronic energy levels in the presence of a weak magnetic field [~~10~~14], which in our case implies a kind of topological Zeeman effect for the axial refractive indices of the modes in the twisted fibers. Because in the experiments the twist period is large compared to the transverse period and the core diameter of the PCF, the physical system can be modeled by perturbation theory similar to that used in quantum mechanics.

The axis of an optical fiber defines the direction of translational invariance along which the optical modes propagate. A general electromagnetic field can be decomposed into a set of such modes (both free and bound) with known transverse field profiles and effective phase indices along this axis [~~11~~10]. Translational invariance can still be maintained in a continuously twisted fiber if a helicoidal coordinate system, twisting with the fiber structure, is used. This makes it possible to decompose the electromagnetic field into a new set of helicoidal fiber modes.

The topological Zeeman effect lifts the degeneracy of predominantly left (LC) and right (RC) circularly polarized modes, giving rise to the appearance of circular birefringence in PCFs twisted around their central axis (inset of Fig. 1). As mentioned also in [~~5~~4], care must be taken because the topological Zeeman effect is described in the twisted (not the laboratory) coordinate frame. We show that the axial refractive indices must be transformed back into the laboratory frame if the circular birefringence is to be correctly predicted. We observe good agreement between experimental data, numerical calculations, and perturbation theory for the structure treated—an endlessly single-mode (ESM) PCF [~~12~~15].

Untwisted optical fibers

Conventional optical fibers possess a direction of translation invariance, which we define as the z axis of a cartesian coordinate frame Oxyz. Furthermore, it is convenient to express the transverse coordinates x and y in terms of cylindrical coordinates ρ and ϕ, with $x = \rho\cos\phi$ and $y = \rho\sin\phi$, where $\rho = 0$ defines the center of the fiber.

For the sake of convenience we formulate Maxwell's equations in the frequency domain, the time dependence $\exp(-i\omega t)$ being understood. Owing to the direction of translation invariance, the permittivity

and permeability tensors are functions only of ρ and ϕ, which allows Maxwell's equations to be significantly simplified. The complexity of the resulting equations can be further reduced by additional assumptions such as the paraxial approximation [3]. In this letter, in contrast to these approximate approaches, we present a general and rigorous derivation that can be easily extended to twisted fibers. To this end, we follow the concept in [~~13~~16], where a general eigenvalue equation was developed in Fourier space for arbitrary material tensors. In this letter we adapt the formulation to a twisted frame in real space.

Starting from Maxwell's equations it is possible to derive a matrix operator equation in the following form (see [~~13~~16] and references therein):

$$-i\frac{\partial \mathbf{F}}{\partial z} = M_0(\rho,\phi)\mathbf{F} \ . \qquad (1)$$

Field Code Changed

In this equation, **F** denotes a four-dimensional vector containing the two transverse field components of both the electric and magnetic field **E** and **H**. Note that in Eq. (1) the basis of the underlying Euclidean three-dimensional space $\mathbb{R}^3$ is not fixed, i.e., it may be cartesian, cylindrical or any other convenient system, whereas the spatial coordinates are defined without the loss of generality by coordinates ρ, ϕ, and z.

The 4×4 dimensional matrix operator M_0 on the right hand side of Eq. (1) contains derivatives with respect to the transverse coordinates ρ and ϕ, but is independent of z. As an example, M_0 is expanded in the appendix for isotropic materials by circular polarization states with basis vectors $\mathbf{e}_{LC} = (\mathbf{e}_x + i\mathbf{e}_y)/\sqrt{2}$ and $\mathbf{e}_{RC} = (\mathbf{e}_x - i\mathbf{e}_y)/\sqrt{2}$. Owing to the peculiar form of M_0, equation (1) can be solved via the Ansatz $\mathbf{F}(\rho, \phi, z) = \exp(i\kappa z)\ \mathbf{f}(\rho, \phi)$, which sets up an equation for the eigenvalues κ and eigenmodes **f** of matrix M_0.

In some cases, e.g., for isotropic materials, we can eliminate either **E** or **H** and reduce the dimensionality of the eigenvalue problem by a factor of two, leading for homogeneous materials to the Helmholtz equation. The use of the 4×4 matrix M_0 is however very convenient for treating chirality, such as appears in chiral bi-isotropic materials and twisted systems. Although one could treat also twisted systems with more complex material properties, for the sake of simplicity and clarity we restrict further discussion to lossless isotropic materials.

Let us now consider fibers that are invariant under rotations around the z axis. In this case the z component of the total angular momentum operator, denoted simply by J, and the matrix operator M_0, possess a common set of eigenstates.

Using a circular polarization basis with basis vectors $\mathbf{e}_{LC} = (1,0)^T$ ~~$\mathbf{e}_{LC} = (1,0)^T$~~ and $\mathbf{e}_{RC} = (0,1)^T$ ~~$\mathbf{e}_{RC} = (0,1)^T$~~, the operator J becomes:

$$J = L + S = -i\frac{\partial}{\partial \phi} + \begin{pmatrix} 1 & 0 \\ 0 & -1 \end{pmatrix}. \qquad (2)$$

Formatted: Font: 12 pt, Bold
Formatted: Font: Italic, Subscript
Formatted: Superscript
Formatted: Font: 12 pt
Field Code Changed

This operator is diagonal with eigenvalues j, which provide the total angular momentum number and are doubly degenerate. Possible eigenstates are $\exp(il_-\phi)\mathbf{e}_{LC}$ ~~$\exp(il_-\phi)\mathbf{e}_{LC}$~~ and $\exp(il_+\phi)\mathbf{e}_{RC}$ ~~$\exp(il_+\phi)\mathbf{e}_{RC}$~~, where $l_\pm = j \pm 1$ denotes the orbital angular momentum number, which is an integer due to the azimuthal resonance condition. Assigning spin numbers $s = 1$ for LC and $s = -1$ for RC polarized eigenstates, we note that $j = l + s$. Solutions of Maxwell's equations consist of special linear combinations of these degenerate eigenstates [~~11~~10], where each eigenstate is weighted with a radially dependent function $f_j(\rho)$. The integer value j is often referred to as the azimuthal mode order. For each azimuthal mode order, Maxwell's equations provide an infinite number of solutions, differing in their radial dependence by radial mode order p, which is a positive integer. The fundamental modes are doubly degenerate with $|j| = 1$ and $p = 1$, which means that any linear combination of them will also yield a fundamental mode. Typically, they are chosen to be linearly polarized along the x and y directions at the fiber center and labeled HE_{11}^o and HE_{11}^e, where the superscripts e and o denote even and odd y-distributions of the x component of the electric field across the xz plane. As we will show later, it is more convenient for twisted fibers to consider linear combinations which are LC and RC polarized at the fiber center, because the twist breaks the modal degeneracy into LC and RC polarized branches.

It is worth mentioning that, even in the simple case of rotational invariance, solutions of Maxwell's equations are in general not perfectly LC or RC polarized, but rather contain a mixture of both spin states corresponding to orbital angular momentum numbers $l_\pm = j \pm 1$. The fundamental fiber modes, however, are predominantly LC ($j = 1$) and RC ($j = -1$) polarized, with $l \approx 0$ and an intensity maximum at the fiber center. In contrast, higher order fiber modes with $|j| \neq 1$ contain larger orbital angular momentum (OAM) contributions and are therefore confined in concentric rings around the core center.

Although rotational invariance is broken in ESM-PCF, six-fold rotational symmetry is still preserved. In addition, most PCFs belong to the symmetry group C_{6v}, i.e., they possess additionally mirror symmetry. The absence of rotational invariance means that solutions of Maxwell's equations have to be constructed by a superposition of J eigenstates, the six-fold rotational symmetry imposing some restrictions on the modes. In particular, perfect six-fold rotational symmetry allows six different classes of modes to be distinguished, each class consisting of a superposition of J eigenstates with eigenvalues $j_0 + 6m$ for integer values j_0 and m. When these modes are rotated by 60° they reproduce themselves perfectly except for a phase term $\exp(ij_0\pi/3)$. Note that the fundamental order j_0 is not defined uniquely; usually it is restricted to $j_0 = -2, -1, 0, 1, 2, 3$, which sets up the first azimuthal Brillouin zone.

The lower order core modes in PCF resemble with good accuracy the modes of rotationally invariant fibers [~~13~~12, ~~14~~13], so that it is convenient to define j_0 as the dominant J contribution to the mode and omit the subscript for the sake of simplicity. Although in this sense values of j_0 outside the first azimuthal Brillouin zone may be allowed, this is not usually of interest in standard PCFs due to the high loss of such modes. For this reason the more complicated case of cladding modes and higher order core modes is

Formatted: Font: Italic
Formatted: Font: Italic, Subscript
Formatted: Font: Symbol, Italic
Formatted: Font: 12 pt, Bold
Formatted: Font: Italic, Subscript
Formatted: Font: Italic
Formatted: Font: Italic, Subscript
Formatted: Font: Symbol, Italic
Formatted: Font: 12 pt, Bold
Formatted: Font: Italic, Subscript

beyond the scope of this paper. Moreover, in the following analysis we restrict the radial mode order to unity and label modes simply by the dominant total angular momentum number j.

With regard to the degeneracy of modes in untwisted PCFs, it has been shown that those modes which obey the full symmetry of the fiber are non-degenerate ($j - 6m = 0, 3$), whereas other modes are twice degenerate [~~14~~12,~~15~~13]. Furthermore, degenerate modes possess identical radial mode orders and dominant azimuthal mode orders of the same magnitude but opposite sign.

Twisted fibers

When twisting fibers around their center with axial twist period Λ and twist rate $\alpha = 2\pi/\Lambda$, the fiber axis as the direction of light propagation is no longer a direction of translational invariance. However, the twisted system still possesses a direction of translational invariance along the helical path of the twisted coordinate frame. The change from untwisted to twisted fiber can be formally described by $M_0(\rho,\phi) \rightarrow M_0(\rho,\phi+\alpha z)$. We can therefore introduce a coordinate transformation from the laboratory frame to the twisted coordinate frame [1,4,~~16~~17], thus bringing Maxwell's equations into the form of Eq. (1).

The most elegant way to describe the coordinate transformation is to view the z component of the total angular momentum operator as the generator of rotations [~~10~~14]. Thus, over a propagation distance z (rotation angle αz) the matrix M_0 obeys the following transformation rule:

$$\exp(-i\alpha z J) M_0(\rho,\phi+\alpha z) \exp(i\alpha z J) = M_0(\rho,\phi) \ . \qquad (3)$$

Field Code Changed

Note that M_0 on the left-hand side is defined in the laboratory frame, whereas M_0 on the right-hand side denotes the matrix in the twisted coordinate frame. Substituting $\mathbf{F}$ into Eq. (1) using $\mathbf{F}_\alpha = \exp(i\alpha z J)\mathbf{G}_\alpha$ and Eq. (3) yields:

$$-i\frac{\partial \mathbf{G}_\alpha}{\partial \zeta} = \left[M_0(\rho,\theta) - \alpha J\right]\mathbf{G}_\alpha \ . \qquad (4)$$

Field Code Changed

So as to avoid any confusion regarding the cartesian laboratory frame and the twisted coordinate frame, we have formally replaced z by ζ and ϕ by θ in Eq. (4), where $\zeta \rightarrow \zeta + \Delta\zeta$ denotes shifts along the direction of translational invariance of the twisted fiber and θ is the azimuthal angle in the twisted coordinate frame. Equation (3) can be solved in the same manner as Eq. (1) via the Ansatz $\mathbf{G}_\alpha = \exp(i\kappa_\alpha \zeta)\mathbf{g}_\alpha$. $\mathbf{G}_\alpha$ is then a solution defined in the twisted coordinate frame, corresponding to a twist rate α. It is worth mentioning that so far no approximation has been made in deriving Eq. (4), so that precise numerical solutions for $\mathbf{G}_\alpha$ can be calculated by methods such as finite-element modeling [1,4,~~16~~17]. Moreover, owing to our use of four-component vectors $\mathbf{G}_\alpha$ containing all four transverse field components (electric and magnetic), the total angular momentum operator J contributes only linearly to the modified eigenvalue equation. If we had used just the two transverse electric field components, described by two-component vectors, J would have contributed quadratically to the eigenvalue equation [18].

Formatted: Font: Bold

Formatted: Font: Symbol, Italic, Subscript

Formatted: Font: Italic

Formatted: Font: Italic

Evidently a formal analogy exists between Maxwell's equations in a twisted coordinate frame and the Pauli equation for electrons in the presence of weak magnetic fields [~~10~~14], so that we can expect κ_α to depend on α in a manner similar to Zeeman splitting of energy levels in quantum mechanics (note however that the electronic wave-function is a two-dimensional vector in the spin-up and spin-down basis, in contrast to the four-dimensional vectors $\mathbf{G}_\alpha$). In fact, the angular momentum operator in Eq. (4) should be a four-dimensional matrix operator, denoted by the Kronecker product as $1_{2\times2} \otimes J$, so as to agree with the standard convention of quantum mechanics, where J is a 2×2 matrix. In this sense, equation (4) more closely resembles the four-dimensional Dirac equation, with counter-propagating modes as the corresponding anti-particles, since the role of time and space is inverted in optics compared to the equations of quantum field theory.

After twisting the fiber around its axis, rotational symmetry is maintained, so that we can still assign radial and azimuthal mode orders p and j to the fiber modes. For systems with broken rotational invariance, the fiber twist introduces additionally a weak periodic modulation along the fiber axis, which implies for six-fold symmetric PCFs that the fiber modes reproduce themselves after translations by $\Delta z = \pi/3\alpha$ along the z axis, except for a Bloch phase term $\exp(i\beta_\alpha \Delta z)$. Note that, like the azimuthal mode order, the phase β_α is not unique, because multiples of 6α can be added to it without changing the phase.

Perturbation theory

In many practical applications, the twist rate α is comparatively small, which means that the twist period Λ is much longer than the relevant transverse length-scales. As a consequence, equation (4) can be solved approximately using a perturbation approach, where αJ provides only a minor correction to the eigenvalues of M_0. The general treatment follows that used for the Zeeman effect [~~10~~14], except that the underlying overlap integrals are different. Let us assume that known solutions of Maxwell's equations for the untwisted problem are:

$$\kappa_0 \mathbf{g}_0 = M_0 \mathbf{g}_0 . \tag{5}$$

Since the amplitude of the modes $\mathbf{g}_0$ is not fixed in Eq. (5), it is useful to carry out a suitable normalization. We choose to normalize the power as the integrated time-averaged z component of the Poynting vector [in cartesian basis and cgs units: $S_z = \left(E_x H_y^* - E_y H_x^*\right) c / 8\pi$, where the asterisk denotes the complex conjugate] to its value at $\zeta = 0$, which is a conserved quantity for truly guided modes, but ζ-dependent otherwise. Formally we can define the normalization for forward propagating modes as $\langle g | i\gamma | g \rangle = 1$, where γ is a 4×4 matrix that depends on the underlying coordinate system used. In a circular polarization basis, γ equals the Dirac matrix γ^3; in a cartesian basis, it equals γ^2 (see appendix). In general, the appropriate overlap integral for vectors $\mathbf{g}$ and $\tilde{\mathbf{g}}$ ~~$-\tilde{\mathbf{g}}$~~ can be written as

$$\langle \tilde{g} | i\gamma | g \rangle = \frac{c}{16\pi} \iint \mathrm{d}A \tilde{\mathbf{g}}^\dagger i\gamma \mathbf{g} \quad \langle \tilde{g} | i \quad | g \rangle - \frac{c}{16} \quad \mathrm{d}A \tilde{\mathbf{g}}^\dagger i \quad \mathbf{g}, \tag{6}$$

Field Code Changed

Field Code Changed

Field Code Changed

Field Code Changed

where the integral is taken over the area normal to the fiber axis and $\tilde{\mathbf{g}}^{\dagger}$ denotes the conjugate transpose of $\tilde{\mathbf{g}}$. One can easily confirm in a cartesian basis that this leads to power normalization for identical vectors $\mathbf{g}$ and $\tilde{\mathbf{g}}$. This form of normalization is useful not only for relating the electric and magnetic field to the power, but also is connected to other important integral quantities [17,19]. For example, $\langle J\rangle = \langle g|i\gamma J|g\rangle$ equals the z component of the normalized total angular momentum flux. In addition, we can separate the spin and orbit contributions by splitting J into its spin and orbit part as $J = S + L$ and calculating the overlap integrals for the individual contributions, i.e., $\langle L\rangle = \langle g|i\gamma L|g\rangle$ and $\langle S\rangle = \langle g|i\gamma S|g\rangle$. More details are provided in the appendix. Furthermore, in the case of fully bound modes, it is possible to obtain the power orthogonality relation $\langle \tilde{g}_0|i\gamma|g_0\rangle = 0$ for $\tilde{g}_0 \neq g_0$ [10,18,20].

In linear perturbation theory, we assume that a general solution $\mathbf{g}_\alpha$ of the twisted system can be written (using power-flux normalized vectors) as $\mathbf{g}_\alpha \approx \mathbf{g}_0$. In other words, within this approximation, twisting the fiber simply forces the field distributions of the untwisted fiber to follow the fiber twist. After multiplying Eq. (4) from the left with $\mathbf{g}_0^{\dagger}\exp(-i\kappa_\alpha\zeta)i\gamma$ and integrating over the transverse area, the approximate eigenvalues of the twisted fiber take the form:

$$\kappa_\alpha \approx \kappa_0 - \alpha\langle J\rangle. \tag{7}$$

A direct consequence of approximating the modes of the twisted fiber with those of the untwisted fiber is that perturbations of higher than linear order are neglected. This works well unless the modes of the untwisted system are degenerate (e.g., for the fundamental core modes), in which case we have to find a special linear combination of the degenerate solutions, for which the perturbation operator J is diagonalized in the subspace of the degenerate solutions [10,14].

For fibers with rotational symmetry, one can deal with this problem by constructing the modes as eigen-solutions of J. Since PCFs have six-fold rotational symmetry, degenerate states are associated with azimuthal mode orders of the same magnitude but opposite sign. Owing to the restriction of degenerate modes to orders $j \neq 0, \pm 3, \pm 6, \ldots$, it is possible to show that the overlap integral of J eigenstates equals zero for degenerate pairs of modes with orders $\pm j$:

$$\left\langle g_0^{\mp j}\middle|i\gamma J\middle|g_0^{\pm j}\right\rangle = \left\langle g_0^{\mp j}\middle|\exp(-iJ\pi/3)i\gamma J\exp(iJ\pi/3)\middle|g_0^{\pm j}\right\rangle = e^{\pm 2ij\pi/3}\left\langle g_0^{\mp j}\middle|i\gamma J\middle|g_0^{\pm j}\right\rangle = 0\ . \tag{8}$$

The last equality sign on the right-hand side is a direct consequence of $\exp(\pm 2ij\pi/3) \neq 1$ for degenerate states with $j \neq 0, \pm 3, \pm 6, \ldots$. This defines the appropriate basis of eigenstates for degenerate perturbation theory. Moreover, in the case of C_{6v} symmetry, $\left\langle g_0^{j}\middle|i\gamma J\middle|g_0^{j}\right\rangle = -\left\langle g_0^{-j}\middle|i\gamma J\middle|g_0^{-j}\right\rangle$.

In the numerical calculations that follow, the fiber parameters are those previously reported [3]. The PCF has a hexagonal array of hollow channels arranged in a pattern of five rings around a central solid glass

Field Code Changed
Field Code Changed
Field Code Changed
Field Code Changed
Field Code Changed
Field Code Changed
Field Code Changed
Field Code Changed

core. The inter-hole period is 2.914 µm and the radius of the air holes (refractive index 1.0) is 0.552 µm. The dispersion of the fused silica is modeled using the well-known Sellmeier expansion [~~19~~21].

Figure 1 shows the effective index splitting ($n_{\text{eff}} = \kappa_\alpha / k_0$ with k_0 as the vacuum wave number) of the fundamental core modes of this fiber at a wavelength of 800 nm. The red and blue solid lines show numerically exact results calculated using a commercial finite-element solver (JCMwave with twisted coordinate frame implemented as in [~~16~~17]). The insets on the left-hand side show the corresponding z-component of the spin angular momentum density for zero twist [~~17~~19], which provides the local degree of circular polarization. After integration over the density, we obtain $\langle S \rangle = \pm 0.9996$, $\langle L \rangle = \pm 0.0021$, and $\langle J \rangle = \pm 1.0017$ for the spin, orbital, and total angular momentum. We note that the magnitude of $\langle S \rangle$ differs slightly from unity, which means that the core modes are not perfectly LC or RC polarized. The black dots in Fig. 1 are the result of perturbation theory analysis, and are in good agreement with the numerical results. We can clearly see the expected predominantly linear mode splitting in the numerical results.

Circular birefringence of fiber modes

From these results it is clear that perturbation theory yields accurate solutions for twisted fibers, a large refractive index splitting (between predominantly LC and RC polarized modes) appearing in the twisted frame, suggesting the presence of circular birefringence. The analysis would predict the same result in rotationally invariant fibers, which is quite clearly incorrect. It is clear therefore that the coordinate transformation itself generates the index splitting. This makes sense, for in order for a linear polarized azimuthal field pattern to be preserved in the laboratory frame as it travels, it must consist of the superposition of two spin angular momentum modes of equal and opposite order but different effective indices in the twisted frame. We now show how to separate this "geometrical" effect from the real measurable circular birefringence that can occur in twisted PCFs in the laboratory frame.

To study circular birefringence it is most efficient to describe the fields in a circular polarization basis. Let us consider fiber modes $\mathbf{G}_\alpha^j$ described in the twisted coordinate frame. These modes have a global phase κ_α^j for translations along the helical path as the direction of invariance, but possess also special rotation properties denoted by the azimuthal mode order j. Taking into account the generator of rotations in the circular polarization basis defined in Eq. (2), we can generally use the following Ansatz:

$$\begin{pmatrix} G_{\alpha,LC}^j \\ G_{\alpha,RC}^j \end{pmatrix} = e^{i\kappa_\alpha^j \zeta} \sum_m \begin{bmatrix} e^{i(j+6m-1)\theta} g_{\alpha,LC}^{jm}(\rho) \\ e^{i(j+6m+1)\theta} g_{\alpha,RC}^{jm}(\rho) \end{bmatrix}. \tag{9}$$

Note that $G_{\alpha,LC/RC}^j$ denotes the transverse field components of either the electric or the magnetic field. The sum on the right-hand side is taken over the different J eigenstates contributing to this particular mode, with radial dependence $g_{\alpha,LC/RC}^{jm}(\rho)$ and order $j+6m$. Note that the $g_{\alpha,LC/RC}^{jm}(\rho)$ elements can be derived by evaluating the azimuthal Fourier transform of the power-flux normalized eigenstate $\mathbf{g}_\alpha^j(\rho,\phi)$. They

Field Code Changed

Field Code Changed

Field Code Changed

therefore depend on the twist rate α, and their absolute magnitude decreases as $|m|$ increases. Transforming these modes into the laboratory frame we find:

$$\begin{pmatrix} F^j_{\alpha,LC} \\ F^j_{\alpha,RC} \end{pmatrix} = \exp(i\alpha z J) \begin{pmatrix} G^j_{\alpha,LC} \\ G^j_{\alpha,RC} \end{pmatrix} = e^{i\kappa^j_\alpha z} \sum_m \begin{bmatrix} e^{i(j+6m)(\phi+\alpha z)-i\phi} g^{jm}_{\alpha,LC}(\rho) \\ e^{i(j+6m)(\phi+\alpha z)+i\phi} g^{jm}_{\alpha,RC}(\rho) \end{bmatrix}. \quad (10)$$

Evidently, each set of total angular momentum states progresses in the laboratory frame with a propagation constant $\beta^{jm}_\alpha = \kappa^j_\alpha + \alpha(j+6m)$. Using Eq. (7) to obtain approximate expressions for β^{jm}_α yields:

$$\beta^{jm}_\alpha = \kappa^j_\alpha + \alpha(j+6m) = \kappa^j_0 - \alpha(\langle J\rangle - j - 6m) + O(\alpha^2). \quad (11)$$

Note that we have introduced here an additional correction term of order α^2, which takes into account higher order corrections in cases where the term linear in α becomes small.

In the case of fibers with rotational invariance, each eigenstate of the untwisted fiber can be chosen such that it contains only one total angular momentum eigenstate, i.e., $m = 0$ in Eq. (11). Furthermore, these eigenstates are also exact solutions of the twisted eigenvalue problem of Eq. (4), with $\langle J\rangle = j$, so that $\beta^{j0}_\alpha = \kappa^j_0$. This is the mathematical proof that twisting has no effect in rotationally invariant systems, when the circular birefringence is zero.

If we consider PCFs with six-fold symmetry, as stated above, there are pairs of degenerate modes in the untwisted fiber, which we label by integers $\pm j$ according to their azimuthal mode orders. The corresponding expectation values of the total angular momentum will be denoted $\langle J\rangle_\pm$. Keeping in mind that eigenstates with positive/negative j are usually predominantly LC/RC polarized, each pair of total angular momentum states with total angular momentum numbers $\pm(j+6m)$ will exhibit circular birefringence $B^m_C = \alpha(\langle J\rangle_+ - \langle J\rangle_- - 2j - 12m)/k_0$. Because modes with larger values of m usually contain larger OAM contributions, their intensity maxima are located in rings surrounding the fiber axis. The observable circular birefringence will therefore depend on the radial position of the mode in the fiber. In addition, most of the power is usually carried by only a few angular momentum orders.

In the case of the fundamental core modes, the strongest contribution is the order $m = 0$, which in the example PCF carries more than 98% of the modal power, meaning that all other contributions can be considered as only minor corrections when measuring the circular birefringence. The normalized intensity distributions of the m = −1, 0, 1 contributions to the predominantly LC polarized core mode of the untwisted ESM fiber are depicted in Fig. 2. Each row of panels shows one particular value of m, the overall intensity being shown in the left-hand column and the corresponding LC and RC polarized intensity in the other columns. As expected, the RC polarized contribution to the $j = 1$ state can be neglected. Similarly, the $m \neq 0$ states play a minor role. This can be also seen in Fig. 3, where the normalized power of several total angular momentum contributions is shown for the predominantly LC polarized mode. In agreement with the symmetry considerations above, only those orders differing from

Formatted: Font: Symbol, Italic
Formatted: Font: Italic
Field Code Changed
Field Code Changed
Field Code Changed

$j = 1$ by multiples of six contribute significantly to the predominantly LC polarized mode, their amplitudes decreasing with increasing $|m|$. All other contributions can be considered as numerical noise.

When we make use of the C_{6v} symmetry of the fiber, the final result for the circular birefringence simplifies further, because in this case $\langle J \rangle_+ = -\langle J \rangle_- \equiv \langle J \rangle$, which leads for $m = 0$ to:

$$B_C = n_{RC} - n_{LC} = \alpha\left(\langle J \rangle - j\right)\lambda / \pi \,. \qquad (12)$$

Field Code Changed

Field Code Changed

Field Code Changed

After a distance Δz, this rotates a launched linear polarization by $\Delta\varphi = \pi B_C \Delta z / \lambda = \alpha\left(\langle J \rangle - j\right)\Delta z$. We note that a non-vanishing circular birefringence requires $\langle J \rangle \neq j$, which in turn means that the power carried in orders $j + 6|m|$ is not equal to that carried by orders $j - 6|m|$. It is this small asymmetry that causes a measurable and reproducible optical activity [3].

Figure 4 shows the α-dependence of the circular birefringence in the example PCF calculated both numerically (green solid line) and using perturbation theory (black dotted line). The experimental data points are also included (red squares). The overall agreement is excellent, the blue solid line showing the small disparity between numerical calculation and perturbation theory.

It is interesting to note that the circular birefringence of twisted fibers can be successfully modeled by linear perturbation theory, even though $\left|\langle J \rangle - j\right|$ is rather small (≈ 0.0017). For the example PCF it turns out that linear perturbation theory is, however, inadequate for describing the effective index of the $m = 0$ contribution in the laboratory frame, where quadratic behavior is dominant (Fig. 5). Only when zooming into the region of very small twist rates does the linear regime dominate (inset of Fig. 5). It may appear surprising that linear perturbation theory reproduces the exact results for the circular birefringence so well. The reason is that a quadratic perturbation term does not depend on the sign of the azimuthal mode order j. For the fundamental fiber mode, it always increases the index. Moreover, due to C_{6v} symmetry, the quadratic contributions to the circular birefringence cancel out completely. The next perturbation term with a polarization dependent influence on the effective index would be the α^3 term, which can be assumed to be much smaller than the term linear in α. In addition, the contribution linear in α is fully real, implying that the circular birefringence is accompanied only by negligible circular dichroism, originating from higher order terms. Only at resonant wavelengths (where the fundamental core modes couple to leaky ring modes in the cladding with larger OAM values [1]) does the circular dichroism become significant. Note that we have included the quadratic term in the theory curve by fitting the quadratic order to the numerical data instead of carrying out a higher order perturbation scheme.

Conclusion

In summary, a perturbation approach allows accurate estimation of the circular birefringence of core modes in twisted fibers. Although a large effective index splitting between RC and LC modes is seen in the twisted fiber frame (a kind of topological Zeeman effect), this almost completely disappears when the

fields are transformed back into the laboratory frame. The final circular birefringence depends on the azimuthal symmetry of the modes and the strengths of the individual higher-order angular momentum contributions. This means that twisted rotationally symmetric fibers do not display any optical activity, whereas twisted PCF does. The optical activity of these fibers can be easily controlled by adjusting the twist rate, which may find applications in polarization control, nonlinear optics and sensing. Finally, it should be mentioned that the presented theory can be easily extended to systems with intrinsic circular birefringence, such as fibers with chiral or magneto-optical materials. Compared to the PCF investigated in this paper, the main difference in such systems is the shift of the modal degeneracy of LC and RC polarized modes to non-zero twist rates.

Appendix

In this section, we provide formulae for the matrix M_0 and the expectation values of $\langle J \rangle$, $\langle L \rangle$, and $\langle S \rangle$ in a circular polarization basis with basis vectors $\mathbf{e}_{LC}$ and $\mathbf{e}_{RC}$. The general vector of transverse field components is defined as $\mathbf{F} = (E_{LC}, E_{RC}, H_{LC}, H_{RC})^{\mathrm{T}}$. The matrix M_0 for isotropic materials becomes:

$$M_0 = ik_0 \begin{pmatrix} \mu & 0 \\ 0 & \varepsilon \end{pmatrix} \gamma^3 + \frac{1}{2k_0} \begin{pmatrix} \nabla_\parallel \varepsilon^{-1} \nabla_\parallel^{\mathrm{T}} & 0 \\ 0 & \nabla_\parallel \mu^{-1} \nabla_\parallel^{\mathrm{T}} \end{pmatrix} \gamma^2, \tag{13}$$

In this case, ε and μ are understood as 2x2 matrices and $\nabla_\parallel \varepsilon^{-1} \nabla_\parallel^{\mathrm{T}}$ as well as $\nabla_\parallel \mu^{-1} \nabla_\parallel^{\mathrm{T}}$ are 2x2 matrices ~~where~~constructed via the outer (vector) product of two-dimensional vectors. In particular, $\nabla_\parallel^{\mathrm{T}} = (\partial_+, \partial_-)$ with $\partial_\pm = \partial/\partial x \mp i\partial/\partial y = \exp(\mp i\phi)(\partial/\partial\rho \mp i/\rho\, \partial/\partial\phi)$ ~~and.~~ The Dirac matrices γ^2 and γ^3 are defined as:

$$\gamma^2 = \begin{pmatrix} 0 & 0 & 0 & -i \\ 0 & 0 & i & 0 \\ 0 & i & 0 & 0 \\ -i & 0 & 0 & 0 \end{pmatrix}, \qquad \gamma^3 = \begin{pmatrix} 0 & 0 & 1 & 0 \\ 0 & 0 & 0 & -1 \\ -1 & 0 & 0 & 0 \\ 0 & 1 & 0 & 0 \end{pmatrix}. \tag{14}$$

After normalizing the field using Eq. (6), the expectation values of orbit, spin, and total angular momentum flux become:

$$\langle L \rangle = \frac{c}{16\pi} \iint \mathrm{d}A \left(-H_{LC}^* \frac{\partial E_{LC}}{\partial \phi} + H_{RC}^* \frac{\partial E_{RC}}{\partial \phi} + E_{LC}^* \frac{\partial H_{LC}}{\partial \phi} - E_{RC}^* \frac{\partial H_{RC}}{\partial \phi} \right),$$

$$\langle S \rangle = \frac{c}{8\pi} \iint \mathrm{d}A \ \mathrm{Im}\left(H_{LC}^* E_{LC} + H_{RC}^* E_{RC} \right), \qquad \langle J \rangle = \langle L \rangle + \langle S \rangle. \tag{15}$$

~~$$\langle L \rangle = \frac{c}{16} \quad \mathrm{d}A \left(\quad H_{LC}^* \quad E_{LC} + H_{RC}^* \quad E_{RC} + E_{LC}^* \quad H_{LC} \quad E_{RC}^* \quad H_{RC} \right),$$~~

~~$$\langle S \rangle = \frac{c}{8} \quad \mathrm{d}A \ \mathrm{Im}\left(H_{LC}^* E_{LC} + H_{RC}^* E_{RC} \right), \qquad \langle J \rangle = \langle L \rangle + \langle S \rangle.$$~~ ~~(15)~~

When using a cartesian instead of a circular polarization basis, we obtain exactly the same integral quantities as in [~~17~~19].

Field Code Changed

Formatted: Font: Symbol, Italic

Formatted: Font: Symbol, Italic

Field Code Changed

Field Code Changed

Field Code Changed

Formatted: MTDisplayEquation

Field Code Changed

Formatted: Normal

Acknowledgment

The UK work was performed as part of our international Max Planck Partnership with the Max Planck Society, supported by SFC, EPSRC and STFC.

References

1. G. K. Wong, M. S. Kang, H. W. Lee, F. Biancalana, C. Conti, T. Weiss, and P. St.J. Russell, "Topological excitation of orbital angular momentum resonances in helically twisted photonic crystal fiber," Science **337**, 446 (2012).
2. W. Shin, Y. L. Lee, B. A. Yu, Y. C. Noh, and K. Oh, "Spectral characterization of helicoidal long-period fiber gratings in photonic crystal fibers," Opt. Commun. 282, 3456-3459 (2009).
3. X. M. Xi, T. Weiss, G. K. L. Wong, F. Biancalana, S. M.Barnett, M. J. Padgett, and P. St.J. Russell, "Optical activity in twisted solid-core photonic crystal fibers," Phys. Rev. Lett. **110**, 143903 (2013).
4. X. Ma, C. H. Liu, G. Chang, and A. Galvanauskas, "Angular-momentum coupled optical waves in chirally-coupled-core fibers," Opt. Express **19**, 26515-26528 (2011).
5. C. N. Alexeyev and M. A. Yavorsky, "Generation and conversion of optical vortices in long-period helical core optical fibers," Phys. Rev. A **78**, 043828 (2008).
6. C. N. Alexeyev, T. A. Fadeyeva, B. P. Lapin, and M. A. Yavorsky, "Generation of optical vortices in layered helical waveguides," Phys. Rev. A **83**, 063820 (2011).
7. M. Ornigotti, G. Della Valle, D. Gatti, and S. Longhi, "Topological suppression of optical tunneling in a twisted fiber," Phys. Rev. A **76**, 023833 (2007).
8. R. Ulrich and A. Simon, "Polarization optics of twisted single-mode fibers," Appl. Opt. **18**, 2241-2251 (1979).
9. A. J. Barlow, J. J. Ramskovhansen, and D. N. Payne, "Birefringence and polarization mode-dispersion in spun single-mode fibers," Appl. Opt. **20**, 2962-2968 (1981).
9. A. W. Snyder and J. Love, "Optical waveguide theory," (Chapman & Hall 1983).
10.
11. A. W. Snyder and X. H. Zheng, "Optical fibers of arbitrary cross-sections," J. Opt. Soc. Am. A **3**, 600-609 (1986).
10.12. M. Steel, T. P. White, C. M. de Sterke, R. C. McPhedran, and L. C. Botten, "Symmetry and degeneracy in microstructured optical fibers," Opt. Lett. **26**, 488-490 (2001).
11. K. Z. Aghaie, V. Dangui, M. J. F. Digonnet, S. Fan, and G. S. Kino, "Classification of the core modes of hollow-core photonic-bandgap fibers," IEEE Journal of Quantum Electronics **45**, 1192-1200 (2009).
12.13.
13. C. Cohen-Tannoudji, *Quantum mechanics*, (Hermann, 1991).
14. ~~A. W. Snyder and J. Love, "Optical waveguide theory," (Chapman & Hall 1983).~~
15. T. A. Birks, J. C. Knight, and P. St.J. Russell, "Endlessly single-mode photonic crystal fiber," Opt. Lett. **22**, 961-963 (1997).

Formatted: Font: Bold

~~16.~~ L. Li, "Fourier modal method for crossed anisotropic gratings with arbitrary permittivity and permeability tensors," J. Opt. A: Pure Appl. Opt. **5**, 345-355 (2003).

~~17. M. Steel, T. P. White, C. M. de Sterke, R. C. McPhedran, and L. C. Botten, "Symmetry and degeneracy in microstructured optical fibers," Opt. Lett. **26**, 488-490 (2001).~~

~~18.~~16. ~~K. Z. Aghaie, V. Dangui, M. J. F. Digonnet, S. Fan, and G. S. Kino, "Classification of the core modes of hollow-core photonic bandgap fibers," IEEE Journal of Quantum Electronics **45**, 1192-1200 (2009).~~

17. A. Nicolet, F. Zolla, and S. Guenneau, "Geometrical transformations and equivalent materials in computational electromagnetism," Compel **27**, 806-819 (2008).

~~19.~~18. C. N. Alexeyev and M. A. Yavorsky, "Optical vortices and the higher order modes of twisted strongly elliptical optical fibers," J. Opt. A: Pure Appl. Opt. **6**, 824-832 (2004).

~~20.~~19. S. M. Barnett, "Optical angular-momentum flux," J. Opt. B: Quantum Semiclass. Opt. **4**, S7-S16 (2002).

~~21.~~20. R. Sammut and A. W. Synder, "Leaky modes on a dielectric waveguide: Orthogonality and excitation," Applied Optics **15**, 1040-1044 (1976).

~~22.~~21. James W. Fleming, "Dispersion in GeO_2-SiO_2 glasses," Appl. Opt. **23**, 4486-4493 (1984).

Formatted: Font: Bold

List of figure captions

Fig. 1. Effective index splitting of the fundamental core modes calculated for an ESM PCF in the twisted coordinate frame. The detailed fiber parameters are given in the text. The continuous blue curves denote the numerical calculations for RC polarized modes, the red curves for LC modes and the dots are the results of perturbation theory. The insets show the normalized z component of the spin angular momentum density. A schematic of the twisted ESM fiber can be seen in the inset on the right-hand side; note that the twist rate is exaggerated for clarity.

Fig. 2. Normalized z component of the Poynting vector distribution for the different total angular momentum contributions of order $j + 6m$ in the case of the predominantly LC polarized fundamental core mode ($j = 1$) of an untwisted ESM fiber. Each row represents a different value of m. The columns show (from left to right) the overall intensity for order m and the corresponding LC and RC polarized contributions. Each panel denotes an area of 10×10 μm^2 centered around the fiber core. The numbers at the bottom of each panel provide the maximum normalized intensity, which has to be multiplied to the relative color scale on the right hand side. Note that more than 98% of the modal power is carried in the LC polarized $m = 0$ contribution.

Fig. 3. Normalized power of different total angular momentum contributions to the predominantly LC polarized core mode of an ESM PCF. The dominant contribution belongs to $j = 1$, which is also the azimuthal order of this mode. Total angular momentum states with order $j + 6m$ contribute less significantly with increasing magnitude of the integer values m, whereas all other contributions are basically numerical noise.

Fig. 4. Circular birefringence of the fundamental core modes in an ESM fiber. Red squares denote experimental data, green solid line shows numerical calculations, and black dots depict the perturbation theory. The deviation between perturbation theory and numerical calculations is illustrated by the blue solid line corresponding to the right axis. The agreement between theory, numerical data, and experiment is excellent.

Fig. 5. Effective index $n_{\mathrm{eff}}^{\alpha}$ of the dominant total angular momentum contributions to the fundamental core modes of a twisted ESM fiber calculated in the laboratory frame, displayed as the deviation from the effective index n_{eff}^{0} of the untwisted fiber. The labeling of the lines is as for the twisted coordinate frame in Fig. 1. Note the dominant α quadratic behavior in contrast to the linear behavior of the effective indices in the twisted coordinate frame. The linear term becomes important only for very small twist rates (inset) and in calculating the circular birefringence of the fiber, when the quadratic terms of LC and RC polarized modes cancel out. The quadratic term has been included in the theory curve by fitting the quadratic order to the numerical data instead of carrying out a higher order perturbation scheme.

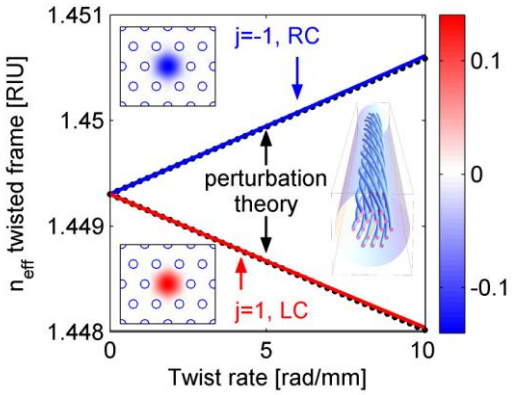

Fig. 1. Effective index splitting of the fundamental core modes calculated for an ESM PCF in the twisted coordinate frame. The detailed fiber parameters are given in the text. The continuous blue curves denote the numerical calculations for RC polarized modes, the red curves for LC modes and the dots are the results of perturbation theory. The insets show the normalized z component of the spin angular momentum density. A schematic of the twisted ESM fiber can be seen in the inset on the right-hand side; note that the twist rate is exaggerated for clarity.

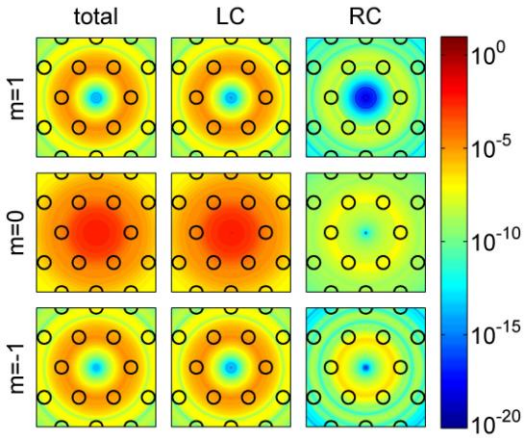

Fig. 2. Normalized z component of the Poynting vector distribution for the different total angular momentum contributions of order $j + 6m$ in the case of the predominantly LC polarized fundamental core mode ($j = 1$) of an untwisted ESM fiber. Each row represents a different value of m. The columns show (from left to right) the overall intensity for order m and the corresponding LC and RC polarized contributions. Each panel denotes an area of 10×10 μm^2 centered around the fiber core. Note that more than 98% of the modal power is carried in the LC polarized $m = 0$ contribution.

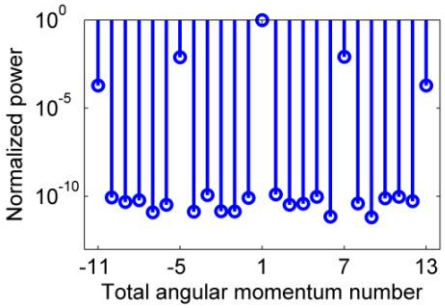

Fig. 3. Normalized power of different total angular momentum contributions to the predominantly LC polarized core mode of an ESM PCF. The dominant contribution belongs to $j = 1$, which is also the azimuthal order of this mode. Total angular momentum states with order $j + 6m$ contribute less significantly with increasing magnitude of the integer values m, whereas all other contributions are basically numerical noise.

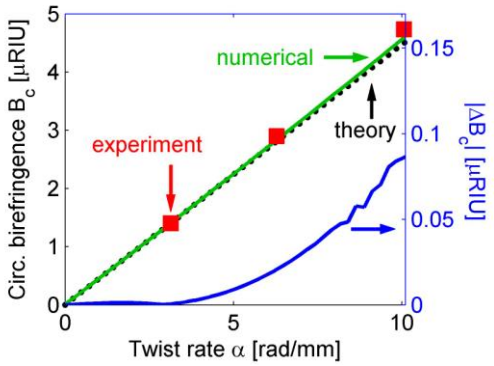

Fig. 4. Circular birefringence of the fundamental core modes in an ESM fiber. Red squares denote experimental data, green solid line shows numerical calculations, and black dots depict the perturbation theory. The deviation between perturbation theory and numerical calculations is illustrated by the blue solid line corresponding to the right axis. The agreement between theory, numerical data, and experiment is excellent.

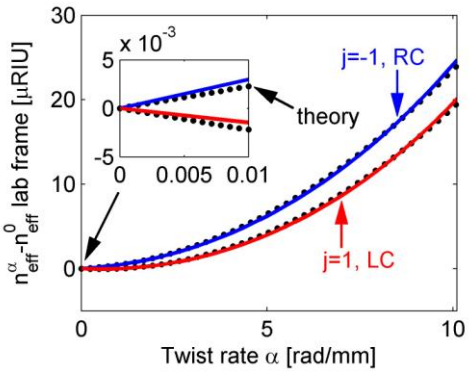

Fig. 5. Effective index $n_{\mathrm{eff}}^{\alpha}$ of the dominant total angular momentum contributions to the fundamental core modes of a twisted ESM fiber calculated in the laboratory frame, displayed as the deviation from the effective index n_{eff}^{0} of the untwisted fiber. The labeling of the lines is as for the twisted coordinate frame in Fig. 1. Note the dominant α quadratic behavior in contrast to the linear behavior of the effective indices in the twisted coordinate frame. The linear term becomes important only for very small twist rates (inset) and in calculating the circular birefringence of the fiber, when the quadratic terms of LC and RC polarized modes cancel out. The quadratic term has been included in the theory curve by fitting the quadratic order to the numerical data instead of carrying out a higher order perturbation scheme.